XIV International Conference on Computational Plasticity. Fundamentals and Applications
COMPLAS XIV
E. Oñate, D.R.J. Owen, D. Peric & M. Chiumenti (Eds)

IDENTIFICATION OF INELASTIC PARAMETERS OF THE 304 STAINLESS STEEL USING MULTI-OBJECTIVE TECHNIQUES

M. VAZ JR. AND M. TOMIYAMA

Department of Mechanical Engineering
State University of Santa Catarina (UDESC)
Campus Universitário Prof. Avelino Marcante, 89219-710 Joinville, Brazil
e-mail: miguel.vaz@udesc.br, masahiro.tomiyama@udesc.br

Key words: Parameter Identification, 304 stainless steel, optimization

Abstract. This work addresses identification of inelastic parameters based on an optimization method using a multi-objective technique. The problem consists in determining the best set of parameters which approximate three different tensile tests. The tensile tests use cylindrical specimens of different dimensions manufactured according to the American ASTM E 8M and Brazilian ABNT NBR ISO 6892 technical standards. A tensile load is applied up to macroscopic failure. The objective functions for each tensile test/specimen is computed and a global error measure is determined within the optimization scheme. The Nelder-Mead simplex algorithm is used as the optimization tool. The proposed identification strategy was able to determine the best set of material parameters which approximate all tensile tests up to macroscopic failure.

1 INTRODUCTION

A proper set of material parameters is one of the most important aspects for a successful simulation of metal forming processes. The present work discusses techniques to obtaining constitutive parameters based on a multi-objective optimization method for the 304 stainless steel. In order to ensure greater generality, the identification strategy is applied simultaneously to tensile tests using specimens of different sizes, defined by the American ASTM E 8M [1] and Brazilian ABNT NBR ISO 6892 [2] standards. The parameter identification method is based on optimization and can approximate the material response up to macroscopic failure with greater accuracy. Noticeably, after the maximum load, the stress state becomes triaxial and the classical calibration techniques cannot be applied.

Identification of elasto-plastic parameters using optimization techniques has long been used in the literature. In the last ten years, many identification strategies have been proposed based on optimization techniques. Most authors agree that the non-linearity of the direct problem (elastoplasticity at finite strains) and the yield curve itself can cause

difficulties in finding the global optimum. A final verdict of best method is temerarious and, so far, the best strategy has proved to be problem dependent. For the sake of objectivity, the reader is referred to Vaz Jr. et al. [3, 4] and references therein for further insights on the application of optimizations techniques to identification of inelastic parameters.

2 PARAMETER IDENTIFICATION AND THE OPTIMIZATION PROBLEM

Parameter identification is a class of inverse problems which determines material or system parameters from a known response. The present problem is formulated using unconstrained optimization and accounts for experimental data obtained from three different tensile tests. Therefore, the multi-objective problem is formulated as

$$\begin{array}{lll} \text{Minimise} & g(\boldsymbol{p}) = \sum_{s=1}^{n_s} \lambda_s g_s(\boldsymbol{p}) & \boldsymbol{p} \in R^{n_d} \\ \text{Such that} & p_i^{\inf} \leq p_i \leq p_i^{\sup} & i = 1, \ldots, n_d \end{array} , \tag{1}$$

where $g(\boldsymbol{p})$ is the objective function (global fitness) of the multi-objective problem, $\boldsymbol{p} = [p_1 \;\; p_2 \;\; \cdots \;\; p_i \;\; \cdots \;\; p_{n_d}]^T$ is the design vector containing n_d material parameters p_i, and $p_i^{\sup}$ and $p_i^{\inf}$ are lateral constraints. The global fitness, $g(\boldsymbol{p})$, comprises contributions from n_s individual problems, so that λ_s is the weight function ($\sum_{s=1}^{n_s} \lambda_s = 1$), and $g_s(\boldsymbol{p})$ is the individual and represents a quadratic relative error measure between the experimental, R_s^{Exp}, and corresponding computed forming load, $R\left(\boldsymbol{p}\right)_s^{Num}$, of a mechanical test "$s$",

$$g_s\left(\boldsymbol{p}\right) = \sqrt{\frac{1}{N_s} \sum_{j=1}^{N_s} \xi_{s,j} \left(\frac{R_{s,j}^{Exp} - R\left(\boldsymbol{p}\right)_{s,j}^{Num}}{R_{s,j}^{Exp}} \right)^2} , \tag{2}$$

in which N_s is the number of experimental points and ξ_s ($0 \leq \xi_{s,j} \leq 1$) is the weight curve of each individual set of experimental data.

The optimization technique adopted in this work uses the gradient-free downhill simplex method, also known as Nelder-Mead algorithm (NM) [5]. The technique defines a regular polytope of $n_d + 1$ vertices (in a n_d dimensional design space), which moves towards the optimum by replacing the worst vertex by a new one selected along a search line. The Nelder-Mead algorithm contains three basic elements: (i) creation of the initial simplex from an initial estimate; (ii) search along a given direction and formation of a new polytope by replacing the worst vertex after the following possible operations: reflexion, expansion, or contraction; and (iii) shrinkage of the polytope towards the best vertex. The reader if referred to References [4, 6, 7] for further insights on the algorithm used in this work.

The Nelder-Mead method has already been used in identification of material constitutive parameters. For instance, Banabic et al. [8] applied to identification of inelastic parameters based on biaxial tensile tests, and Pannier et al. [9] used to find elastic-plastic

constitutive parameters based on the Virtual Fields Method associated to tensile tests. Further details on the application of the NM scheme to mechanical problems are given in Luersen and Le Riche [10]. Noticeably, the authors have already investigated application of the NM scheme for both classical von Mises [4, 6] and damaged materials [7].

3 NUMERICAL RESULTS AND DISCUSSIONS

The identification procedure is based on tensile tests of cylindrical specimens prepared according to the American ASTM E 8M [1] and Brazilian ABNT NBR ISO 6892 [2] technical standards. It is used extensometers with initial gauge length $l_0 = 25$ mm or $l_0 = 50$ mm according to the specimen with maximum crosshead speed 3 mm/min. The specimens used in this work are illustrated in Figure 1 and referred as follows:

- *ASTM #1:* initial gauge length $l_0 = 25$ mm and diameter $d_0 = 6.0$ mm,
- *ASTM #2:* initial gauge length $l_0 = 50$ mm and diameter $d_0 = 12.54$ mm,
- *NBR #3:* initial gauge length $l_0 = 50$ mm and diameter $d_0 = 10.0$ mm,

(a) Specimen *ASTM #1*: $l_0 = 25$ mm, $d_0 = 6$ mm.

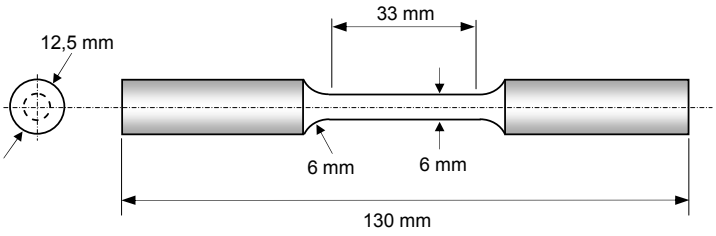

(b) Specimen *ASTM #2*: $l_0 = 50$ mm, $d_0 = 12.54$ mm.

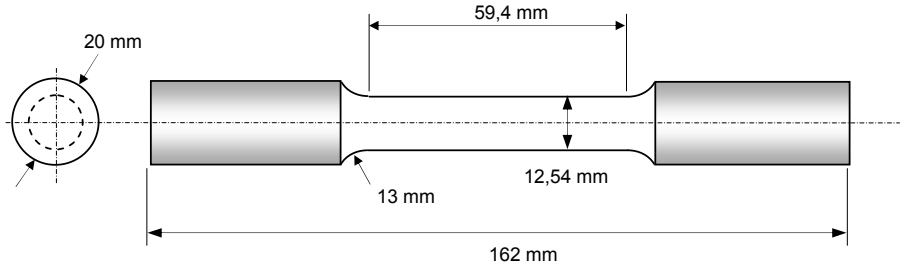

(c) Specimen *NBR #3*: $l_0 = 50$ mm, $d_0 = 10$ mm.

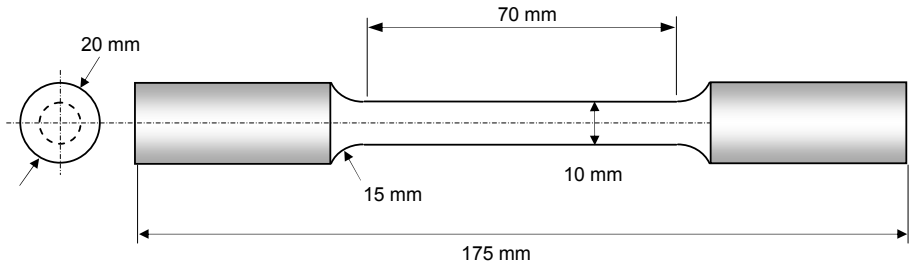

Figure 1: Specimen geometry for ASTM and ABNT-NBR standards.

The finite element mesh used for specimen *ASTM #2* is presented in Figure 2. The geometrical model considers axisymmetry around the rotation axis $Z - Z'$ and symmetry about the $R - R'$ axis, making possible to model only 1/4 of the specimen. It was adopted a structured, eight-noded quadrilateral finite element mesh with 200 elements and 661 nodes with progressive refinement towards the specimen $R - R'$ axis. The meshes used for *ASTM #1* e *NBR #3* specimens were geometrically proportional to *ASTM #2* with identical element topology.

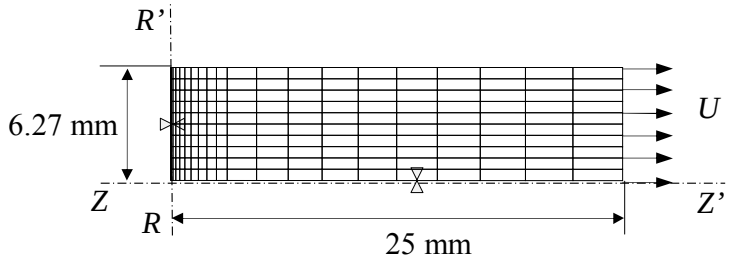

Figure 2: Finite element mesh for the *ASTM #2* specimen.

It is important to highlight that, contrary to the classical calibration procedures, the objective of the present identification process is to determine the material parameters up to macroscopic failure of the specimens. This strategy accounts for larger plastic deformations, making possible to use the material parameters in metal forming processes which present equally large plastic strains. Therefore, instead of using the well-known Swift's [11] equation, this work adopts Voce's [12] modified hardening equation to model isotropic hardening, as

$$\sigma_Y = \sigma_0 + \zeta r + (\sigma_\infty - \sigma_0)\left[1 - \exp\left(-\delta r\right)\right] \ , \tag{3}$$

where σ_0 is the initial yield stress, σ_∞ is the saturation stress, and ζ and δ are the exponential and linear hardening parameters, respectively, so that the parameters to be determined are $\{\boldsymbol{p}\} = \{\sigma_0 \ , \ \sigma_\infty \ , \ \zeta \ , \ \delta\}$.

3.1 The identification process

This section summarises an investigation on convergence aspects of the optimization problem. An initial assessment indicates that the individual (each specimen) and global (combining all specimens) optimization problems are convex, making possible to use the Nelder-Mead optimization scheme. The control parameters for the NM algorithm used in the simulations are $\rho = 1, \gamma = 2, \beta = 0,5$ e $\sigma = 0,5$, whereas the initial estimate and lateral constraints are presented in Table 1.

One can define three basic identification problems according to individual tensile tests. In Case (A) identification is performed taking into account *only* the experimental curve for specimen *ASTM #1*. Cases (B) and (C) are solved in similar fashion, accounting for only experimental curves for specimens *ASTM #2* and *NBR #3*, respectively. Therefore,

Table 1: Lateral constraints and initial estimate.

Parameter p_i	**Lower limit** $p_i^{\inf}$	**Upper limit** $p_i^{\sup}$	**Initial estimate** p_i^0
σ_0 [MPa]	200	800	500
σ_∞ [MPa]	400	1200	800
ζ [MPa]	300	1200	750
δ	0	50	25

identification based on experimental data for specimens *ASTM #1*, *ASTM #2* and *NBR #3* are solved for the following sets of weight parameters, λ_s: Case (A) $\lambda_1^{(A)} = 1.0$ and $\lambda_2^{(A)} = \lambda_3^{(A)} = 0.0$, Case (B) $\lambda_2^{(B)} = 1.0$ and $\lambda_1^{(B)} = \lambda_3^{(B)} = 0.0$, and Case (C) $\lambda_3^{(C)} = 1.0$ and $\lambda_1^{(C)} = \lambda_2^{(C)} = 0.0$.

In addition to the aforementioned cases, in Case (D), identification is also performed assuming that each tensile test imposes the same effect in obtaining the material parameters, i.e. the global objective function, $g(\boldsymbol{p})$, is computed using weights $\lambda_1^{(D)} = \lambda_2^{(D)} = \lambda_3^{(D)} = 1/3$.

Figure 3 shows evolution of the convergence index, $\phi^{(k)} = [g(\boldsymbol{p})_{n_d+1}^{(k)} - g(\boldsymbol{p})_1^{(k)}]/[g(\boldsymbol{p})_{n_d+1}^{(0)} - g(\boldsymbol{p})_1^{(0)}]$, which represents the relative difference between the worst and best vertices of the polytope with respect to the initial simplex. In this work, convergence is assumed for $\phi^{(k)} \leq 10^{-9}$. It can be observed that evolution of the identification process is similar for Cases (A), (B) and (C) and somewhat faster for the equally balanced identification problem, Case (D).

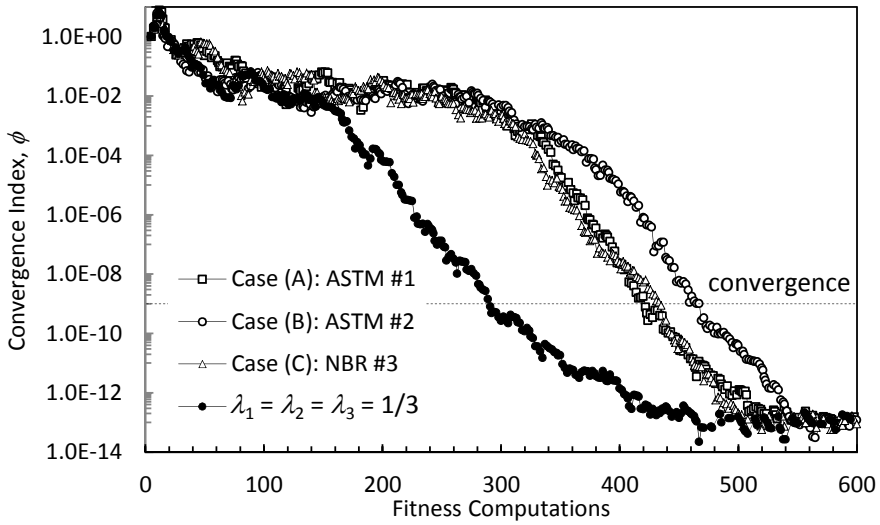

Figure 3: Convergence evolution of the optimization problem.

The Nelder-Mead algorithm requires an initial estimate, from which the initial simplex is constructed. Therefore, the tolerance to changes of the initial estimate yet able to achieve success must also be evaluated. In this case, in addition to the mean values

Table 2: Initial estimates, p_i^0, and final parameters for $\lambda_1 = \lambda_2 = \lambda_3 = 1/3$.

Test	σ_0 [MPa]	σ_∞ [MPa]	ζ [MPa]	δ	**Success?**
Mean	500.00	800.00	750.00	25.0000	Yes
1	200.00	400.40	1084.09	5.0203	Yes
2	638.21	812.33	879.40	0.7273	**No**
3	301.86	1013.47	947.91	7.1787	Yes
4	496.42	1039.51	621.66	6.1902	Yes
5	313.91	614.02	789.68	35.7311	Yes
6	507.68	555.84	696.61	36.4500	Yes
7	509.39	497.26	937.77	19.5037	Yes
8	382.30	504.89	1186.05	27.9432	Yes
9	738.71	766.36	940.71	4.2220	Yes
11	520.93	695.71	958.31	17.6329	Yes
Final Parameters	*399.68*	*686.16*	*878.30*	*9.9677*	

(shown in the last column of Table 1), ten random initial estimates located within the search space are also used. This test was performed for uniform weight parameters ($\lambda_1 = \lambda_2 = \lambda_3 = 1/3$). Table 2 presents the initial estimates, a success indication and final parameters. The simulations show that only one set of initial parameters was not able to obtain the expected results. The reason probably lies on the small value of parameter δ assumed as initial estimate.

3.2 The loading process

The experimental and numerical load curves are shown in Figure 4, from which the three well-known regions can be distinguished: (a) elastic loading, (b) load increase owing to hardening and (c) load decrease due to reduction of the specimen cross-section area. The transition between (b) and (c) is indicated by the maximum load (also known as instability point). Table 3 presents the individual weights, λ_s, and corresponding material parameters for Cases (A)−(D). Case (D) considers that each individual tensile test contributes equally to determine the inelastic parameters.

Table 3: Individual weights, λ_s, and material parameters, $\boldsymbol{p}$.

Case	ASTM #1 $\lambda_1^{(\cdot)}$	ASTM #2 $\lambda_2^{(\cdot)}$	NBR #3 $\lambda_3^{(\cdot)}$	σ_0 [MPa]	σ_∞ [MPa]	ζ [MPa]	δ
(A)	1.0	0.0	0.0	405.89	839.36	714.47	5.3900
(B)	0.0	1.0	0.0	421.45	991.70	372.92	4.6021
(C)	0.0	0.0	1.0	409.16	878.59	597.24	5.1941
(D)	1/3	1/3	1/3	399.68	686.15	878.31	9.9684

Identification for Case (A) requires minimization of the global objective function, $g(\boldsymbol{p})$,

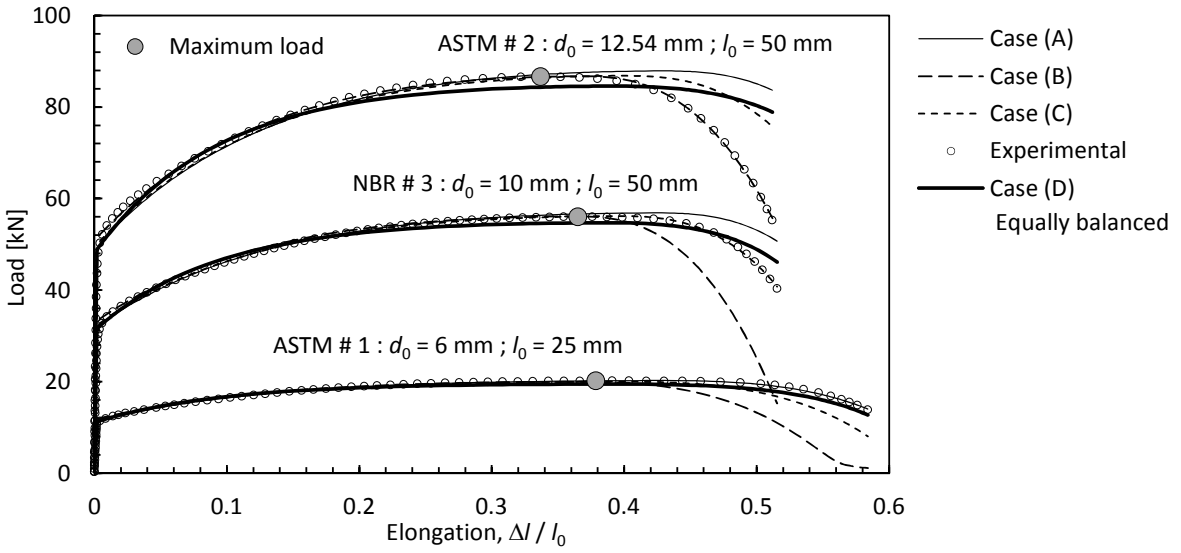

Figure 4: Load curves for tensile tests based on specimens ASTM #1, ASTM #2, and NBR #3.

computed using only the experimental data of specimen ASTM #1 ($\lambda_1^{(A)} = 1.0$, $\lambda_2^{(A)} = \lambda_3^{(A)} = 0.0$). Therefore, the numerical loading curve presents the minimum possible error for specimen ASTM #1, measured by the individual fitness $g_1^{(A)}(\boldsymbol{p}) = 7.2273 \times 10^{-3}$ (the numerical curve visually matches the corresponding experimental data). However, some discrepancies are found when using set (A) of material parameters to simulate tensile tests for ASTM #2 and NBR #3 specimens (the corresponding individual fitness $g_2^{(A)}(\boldsymbol{p}) = 1.4112 \times 10^{-1}$ and $g_3^{(A)}(\boldsymbol{p}) = 5.9591 \times 10^{-2}$).

A similar assessment is also performed for tensile tests of ASTM #1, ASTM #2 and NBR #3 specimens using data sets (B) and (C) of Table 3. Table 4 shows that identification for the corresponding data set yields also very small individual fitness, $g_2^{(B)}(\boldsymbol{p}) = 7.9852 \times 10^{-3}$ and $g_3^{(C)}(\boldsymbol{p}) = 7.9447 \times 10^{-3}$. Nevertheless, as discussed in the previous paragraph, cross-simulations give rise to substantially large individual errors, $g_1^{(B)}$, $g_3^{(B)}$, $g_1^{(C)}$ and $g_2^{(C)}$.

The material data and individual fitness obtained for for Case (D) ($\lambda_1^{(D)} = \lambda_2^{(D)} = \lambda_3^{(D)} = 1/3$) are also presented in Tables 3 and 4. In this case, the numerical curves for ASTM #1, ASTM #2 and NBR #3 specimens present also some differences, especially after the maximum load is reached (see the thick solid line in Figure 4).

The best set of material parameters is not obvious from visual assessment of Figure 4. Furthermore, the differences of the weight parameters, λ_s, for Cases (A)−(D) also preclude use of the global objective function, $g(\boldsymbol{p}) = \sum_{s=1}^{n_s} \lambda_s g_s(\boldsymbol{p})$, to determine the best set of parameters. Therefore, a global index, $G^{(\cdot)}(\boldsymbol{p})$, consisting the mean ratio between the individual fitness and the corresponding minimum value, $g_s^{(\cdot)}/g_s^{min}$, is evaluated as

$$G^{(\cdot)}(\boldsymbol{p}) = \frac{1}{3}\sum_{s=1}^{3} g_s^{(\cdot)}/g_s^{min} \ . \tag{4}$$

Table 4: Individual, $g_s^{(\cdot)}(\boldsymbol{p})$, and relative, $g_s^{(\cdot)}/g_s^{min}$ $^{(*)}$, fitness for Cases (A)−(D).

Case	**Specimen** ASTM#1 $g_1^{(\cdot)}(\boldsymbol{p})$	ASTM#2 $g_2^{(\cdot)}(\boldsymbol{p})$	NBR#3 $g_3^{(\cdot)}(\boldsymbol{p})$	$g_1^{(\cdot)}/g_1^{min}$	$g_2^{(\cdot)}/g_2^{min}$	$g_3^{(\cdot)}/g_3^{min}$	$G^{(\cdot)}(\boldsymbol{p})$
(A)	*7.2273E-03*	1.4112E-01	5.9591E-02	1	17.6721	7.5008	8.7243
(B)	2.9773E-01	*7.9852E-03*	1.5886E-01	41.1946	1	19.9964	20.7303
(C)	1.0617E-01	1.0171E-01	*7.9447E-03*	14.6897	12.7378	1	9.47.58
(D)	3.7466E-02	1.1179E-01	3.1782E-02	5.1839	13.9991	4.0004	7.7278

$^{(*)}$ The minimum individual fitness are $g_1^{min} = g_1^{(A)}$, $g_2^{min} = g_2^{(B)}$ and $g_3^{min} = g_3^{(C)}$.

Table 4 indicates that, based on the global index, Case (D) yields the best numerical approximation to the experimental data of all three tensile tests ($G^{(D)} = 7.7278$). It means that, in average, the error for an individual tensile test is approximately 7.7278 times the minimum possible individual fitness. On the other hand, Case (B) provides the worst set of material parameters with a global index $G^{(B)} = 20.7303$, owing to the excessive load decrease after the maximum load when simulating tensile tests for ASTM #1 and NBR #3 specimens, as shown by the dashed lines in Figure 4.

4 FINAL REMARKS

Hardening parameters for the AISI 304 stainless steel were determined based on three tensile tests using specimens defined by the American ASTM E 8M ($l_0 = 25$ mm, $d_0 = 6.0$ mm, and $l_0 = 50$ mm, $d_0 = 12.54$ mm) [1] and Brazilian ABNT NBR ISO 6892 ($l_0 = 50$ mm, $d_0 = 10.0$ mm) [2] technical standards. The tensile tests were carried out up to macroscopic failure aiming at determining inelastic parameters associated with large plastic strains. The non-uniformity of the stress state after the maximum load precluded application of the classical calibration techniques. Therefore, the identification process used optimization schemes based upon a multi-objective strategy. The global objective function used a weighted combination of individual fitness computed for each tensile test/specimen. The simulations have shown that the size of the specimen plays an important role in the identification problem, thereby requiring a careful balance between effects of individual tensile test/specimen. In the present work, an equally balanced global fitness provided the best approximations for all specimens. However, some differences were observed after the maximum load.

Acknowledgements

The author acknowledges the financial support provided by the Brazilian funding agency CNPq - (National Council for Scientific and Technological Development), grant number 303412/2016-0.

REFERENCES

[1] ASTM - E 8M-86a. Tensile testing of metallic materials. ASTM, Philadelphia (2002).

[2] ABNT NBR ISO 6892. Metallic materials - Tensile testing at ambient temperature. ABNT, Rio de Janeiro (2002).

[3] Vaz Jr. M., Cardoso, E.L., Stahlschmidt, J. Particle swarm optimization and identification of inelastic material parameters *Eng. Comp.* (2013) **30**:936–960.

[4] Vaz Jr. M., Cardoso, E.L., Muñoz-Rojas, P.A., Carniel, T.A., Luersen, M.A., Tomiyama, M., da Silva, J.O., Stahlschmidt, J. and Trentin, R.G. Identification of constitutive parameters - optimization strategies and applications. *Mat.-wiss. u. Werkstofftech.* (2015) **46**:477-491.

[5] Nelder, J.A. and Mead, R. A simplex method for function minimization. *The Comput. Journal* (1965) **7**:308–313.

[6] Vaz Jr., M., Luersen, M. A., Muñoz-Rojas, P. A., and Trentin, R. G. Identification of inelastic parameters based on deep drawing forming operations using a global-local hybrid Particle Swarm approach. *C. R. Mecanique* (2016) **344**:319–334.

[7] Vaz Jr., M., Muñoz-Rojas, P. A., Cardoso, E. L., and Tomiyama, M. Considerations on parameter identification and material response for Gurson-type and Lemaitre-type constitutive models. *Int. J. Mech Sci.* (2016) **106**:254–265.

[8] Banabic D., Kuwabara T., Balan T., Comsa D.S. and Julean D. Non-quadratic yield criterion for orthotropic sheet metals under plane-stress conditions. *Int. J. Mech. Sci.* (2003) **45**:797–811.

[9] Pannier Y., Avril S., Rotinat R. and Pierron F. Identification of elasto-plastic constitutive parameters from statically undetermined tests using the Virtual Fields Method. *Exp. Mech.* (2006) **46**:735–755.

[10] Luersen, M.A. and Le Riche, R. Globalized Nelder-Mead method for engineering optimization. *Comput. & Struct.* (2004) **82**:2251–2260.

[11] Swift, B.H. Plastic instability under plane stress. *J. Mech. Phys. Solids* (1952) **1**:1–18.

[12] Voce, E. The relationship between stress and strain for homogeneous deformation. *J. Inst. Metals* (1948) **74**:537–562.